Biosensors and Bioelectronics 55 (2014) 195–202

Contents lists available at ScienceDirect

Biosensors and Bioelectronics

journal homepage: www.elsevier.com/locate/bios

Sub-femtomolar DNA detection based on layered molybdenum disulfide/multi-walled carbon nanotube composites, Au nanoparticle and enzyme multiple signal amplification

Ke-Jing Huang *, Yu-Jie Liu, Hai-Bo Wang, Ya-Ya Wang, Yan-Ming Liu

College of Chemistry and Chemical Engineering, Xinyang Normal University, Xinyang 464000, China

ARTICLE INFO

Article history:
Received 24 September 2013
Received in revised form
11 November 2013
Accepted 20 November 2013
Available online 7 December 2013

Keywords:
Layered molybdenum disulfide/multi-walled carbon nanotube composites
Au nanoparticle
Glucose oxidase
Multiple signal amplification
DNA biosensor

ABSTRACT

A novel 2-dimensional graphene analog molybdenum disulfide/multi-walled carbon nanotube (MoS_2/MWCNT) was synthesized by a simple hydrothermal method to achieve excellent electrochemical properties. An ultrasensitive electrochemical DNA biosensor was subsequently constructed by assembling a thiol-tagged DNA probe on a MoS_2/MWCNT and gold nanoparticle (AuNP)-modified electrode that has already been coupled with glucose oxidase (GOD). In this work, GOD was used as a redox marker. The heteronanostructure formed on the biosensor surface appeared relatively good conductor for accelerating the electron transfer, while the modification of GOD and AuNPs provided multiple signal amplification for electrochemical biosensing. The multiple signal amplification strategy produced an ultrasensitive electrochemical detection of DNA down to 0.79 fM with a linear range from 10 fM to 10^7 fM, and appeared high selectivity to differentiate three-base mismatched DNA and one-base mismatched DNA. The developed approach provided a simple and reliable method for DNA detection with high sensitivity and specificity, and would open new opportunities for sensitive detection of other biorecognition events.

1. Introduction

Due to the imperative requirements of molecular diagnosis, gene therapy and early screening for tumors, the development of a sensitive strategy for the detection of specific oligonucleotide sequences, especially at low physiological levels, is of great importance (Yin, 2012; Tang et al., 2012; Huang et al., 2011). Different analytical technologies such as chemiluminescence and electrochemistry have been used for DNA detection (Liu et al., 2011; Wang et al., 2013a, 2013b). Electrochemical DNA sensors have received particular interest due to the fact that they can provide a simple, portable, and inexpensive platform for DNA sensing (Wan et al., 2013; Yao et al., 2013). To improve on the sensitivity in the electrochemical detection of DNA, many signal amplification strategies based on the loading of a large number of signal molecules on nanocarrier to label the recognition molecules have been designed (Gao et al., 2013). Nanomaterials can provide a promising sensing platform, because of the high surface areas for enhanced mass transport, the high loading of receptor molecules for synergistic amplification of the target response, and unique electronic and catalytic properties for translating biorecognition events to an electrochemical response. Recently, various nanomaterials, such as metal nanoparticles, metal oxide nanoparticles and semiconductor quantum dots, have been extensively used as signal molecules to significantly enhance the sensitivity and stability due to their unique properties (Wang et al., 2014; Sui et al., 2013; Huang et al., 2013c).

Since their discovery, carbon nanotubes (CNTs) have attracted wide attention in electroanalysis due to their unique properties such as large surface specific area, good mechanical stability, and high electronic conductivity (Karadas et al., 2013). Moreover, CNTs can promote the electron transfer rate between electroactive species and electrodes. Therefore, CNTs have been used as a robust and advanced carbon electrode material for the design of electrochemical sensing platform (Babaei and Taheri (2013); Zhou et al., 2013). Recently, layered transition-metal dichalcogenides (such as WS_2, MoS_2, SnS_2 and VS_2) have attracted more and more attention in the field of electrochemistry due to their large surface specific area and high electronic conductivity (Li et al., 2013; Huang et al., 2013b; Hu et al., 2013; Feng et al., 2011). MoS_2 is a typical family member of transition-metal dichalcogenides. It is composed of Mo metal layers sandwiched between two sulfur layers and stacked together by weak van der Waals interactions (Zhang et al., 2009a, b). The layered structure of MoS_2 is expected to act as an excellent functional material because the 2-dimensional electron–electron correlations among Mo atoms would aid in enhancing planar

* Corresponding author. Tel.: +86 376 6390611.
E-mail address: kejinghuang@163.com (K.-J. Huang).

0956-5663/$ - see front matter © 2013 Elsevier B.V. All rights reserved.
http://dx.doi.org/10.1016/j.bios.2013.11.061

electric transportation properties. Really, MoS_2 has attracted considerable attention due to its extensive applications as catalysts, lubricants, lithium battery, supercapacitor, and so on (Rezaei et al., 2012; Zhang et al., 2009a,b; Hwang et al., 2011; Ma et al., 2013). However, few attentions have been put into its application as an electrode material for sensor because the electronic conductivity of MoS_2 is still lower compared to graphite/graphene (Wang et al., 2013a,b). The combination of MoS_2 and other conducting materials may overcome this deficiency. For example, Ma et al. (2013) have synthesized polypyrrole/MoS_2 composites and used as an advanced electrode material for high-performance supercapacitors applications. Most recently, we constructed a MoS_2-graphene composite based electrochemical sensor and applied to sensitively determine acetaminophen, ascorbic acid and dopamine (Huang et al., 2013a). The MoS_2-graphene based electrochemical method showed informative analytical performance, such as high selectivity, broad dynamic range, and low detection limit.

Here, novel 2-dimensional graphene analog molybdenum disulfide/multi-walled carbon nanotube composites (MoS_2/MWCNT) were synthesized by a simple hydrothermal method to achieve excellent electrochemical properties. A novel reagentless and mediatorless electrochemical biosensor was developed based on the direct electron transfer (DET) of glucose oxidase (GOD) for the detection of specific sequence DNA. Au nanoparticle (AuNP) was firstly immobilized on MoS_2/MWCNT-chitosan composites modified glassy carbon electrode (GCE) surface, and then GOD was immobilized based on Au–thiol interaction. Whereafter, AuNP was deposited on the electrode to act as an electron relay before the specifically designed DNA probe (S1) was attached. GOD was then used to block the remaining active sites. As a redox enzyme, GOD is generally known to exhibit a reversible reaction between its oxidized quinone form (flavin adenine dinucleotide; FAD) and reduced hydroquinone form ($FADH_2$). After the target DNA hybridized with S1 to form double-stranded structure, the DET signal decreased due to the increasing spatial blocking around GOD molecules, giving the quantitative foundation for DNA detection. Herein, upon immobilizing GOD to an AuNP modified MoS_2/MWCNT/GCE, more AuNPs were again attached to the modified electrode and followed by more GOD to introduce signal amplification capability to the biosensor, which would in turn lead to a low detection limit. By integrating MoS_2/MWCNT composites and AuNP signal amplification with enzymatic signal readout, this method showed a sub-femtomolar detection limit of the target DNA with a wide linear range and good selectivity for base discrimination. The designed strategy could be applied to ultrasensitive bioanalysis of DNA.

2. Experimental

2.1. Apparatus

Electrochemical measurements were performed on a CHI 660D Electrochemical Workstation (Shanghai, CH Instruments, China) with a conventional three-electrode system composed of a platinum wire as an auxiliary electrode, a saturated calomel electrode (SCE) as a reference electrode and a 3-mm diameter GCE as a working electrode. The morphologies of the composites were recorded on a JEM 2100 transmission electron microscope (TEM, JEOL, Tokyo, Japan) and a Hitachi S-4800 scanning electron microscope (SEM, Tokyo, Japan). X-ray diffraction (XRD) pattern was operated on a model D/max-rA diffractometer (Rigaku, Japan). Fourier transform infrared spectroscopy (FT-IR) was measured on a Bruker-Tensor 27 IR spectrophotometer (Ettlingen, Germany). Raman spectra were recorded at ambient temperature on a Renishaw Raman system model 1000 spectrometer (Gloucestershire, UK). Thermogravimetric analysis (TGA, SDTQ600, TA Instruments, New Castle DE, USA) was performed under a nitrogen atmosphere at a heating rate of 10 °C min^{-1}.

2.2. Reagents

Graphite powder, $Na_2MoO_4 \cdot 2H_2O$, hydrazine solution (50 wt%) and ammonia solution (28 wt%) were purchased from Shanghai Chemical Reagent Corporation (Shanghai, China). Chitosan (MW 100,000–300,000, deacetylation degree $\geq$95%), chloroauric acid ($HAuCl_4 \cdot 4H_2O$), and the multiwall carbon nanotube (diameter 2–6 nm, length 0.1–10 μm, >90% purity) were purchased from Sigma-Aldrich (St. Louis, USA). The glucose oxidase (GOD) was purchased from Shanghai Sangon Biological Engineering Technology and Services Ltd. (Shanghai, China).

DNA oligonucleotides were purchased from Shanghai Sangon Biological Engineering Technological Co. Ltd. (Shanghai, China). All DNA sequences were synthesized using standard phosphoramidite chemistry and purified using reversed phase high-performance liquid chromatography, and dissolved in 0.01 M phosphate buffered saline (PBS, pH 7.4) with 1 M NaCl before use. Their base sequences are listed below:

Probe ssDNA (S1): 5′-SH-$(CH_2)_6$-TCT TTG GGA CCA CTG TCG-3′;
Target ssDNA (S2): 5′-CGA CAG TGG TCC CAA AGA-3′;
One-base mismatched ssDNA (S3): 5′-CGA CAG TGG TCC CAA CGA-3′;
Three-base mismatched ssDNA (S4): 5′-CGA CAA TGG CCC CAA CGA-3′;
Noncomplementary ssDNA (ncDNA) (S5): 5′-GCA TCG AGC GAG CAC GTA-3′.

2.3. Preparation of Au nanoparticle

AuNP was prepared according to a previous protocol (Jiang et al., 2008). Hundred milliliter 0.01% $HAuCl_4$ solution was boiled with vigorous stirring, and 2.5 mL of 1% trisodium citrate solution was then quickly added to the boiling solution. The solution turned deep red, indicating the formation of AuNP. Upon continued stirring and cooling own, the resulting Au colloidal solution was stored in brown glass bottles at 4 °C before use.

2.4. Synthesis of MoS_2/MWCNT composites

The MoS_2/MWCNT composites were prepared as follows: firstly, 0.017 g MWCNT was ultrasonically dispersed in 40 mL deionized water, and 0.30 g $Na_2MoO_4 \cdot 2H_2O$ was then added and ultrasonically dispersed for 20 min. After adjusting the pH value to 6.5 with 0.1 M NaOH, 0.80 g L-cysteine was added and the mixture was diluted with water to 80 mL, and then the solution was vigorously stirred for about 1 h. After that, the mixture was transferred into a 100 mL Teflon-lined stainless steel autoclave and heated at 180 °C for 48 h. After cooling, the MoS_2/MWCNT composites were collected by filtration, washed with distilled water and absolute ethanol for three times, and dried in vacuum at 80 °C for 20 h. Herein, L-cysteine played a role of reducing agent and sulfur donor during the whole synthesis process, in which L-cysteine released H_2S as a sulfide source as well as a reducing agent, resulting in the reduction of MoO_4^{2-} to MoS_2. The reaction routes could be expressed as follows:

$$HSCH_2CHNH_2COOH + H_2O \rightarrow CH_3COCOOH + NH_3 + H_2S \quad (1)$$

$$4MoO_4^{2-} + 9H_2S + 6CH_3COCOOH \rightarrow 4MoS_2 + SO_4^{2-} + 6CH_3COCOO^- + 12H_2O \quad (2)$$

The MoS_2 was synthesized with the similar procedure in the absence of MWCNT.

2.5. Preparation of DNA biosensor and electrochemical measurements

Chitosan has been widely used for constructing sensors due to its attractive properties including excellent film-forming ability, high permeability, good adhesion and nontoxicity. It also facilitates the electron transfer after its swelling in reaction mixture due to its hydrophilic nature (Ling et al., 2009; Batra and Pundir, 2013). In addition, chitosan has the abundant amino groups and could provide active sites for further AuNP and GOD immobilization.

For electrode preparation, 1 mg MoS_2/MWCNT and 1 mg chitosan was dispersed in 1 mL acetic acid (36%) solution. The GCE was polished carefully with 0.5 and 0.05 μm alumina slurry, and sonicated in ethanol and deionised water, respectively. Then, 8 μL MoS_2/MWCNT-chitosan composites were applied on the pretreated GCE and dried at room temperature to obtain the modified electrode MoS_2/MWCNT/GCE. Afterwards, The MoS_2/MWCNT/GCE was incubated in AuNP (3 mL, 2.5 nM) for 6 h at room temperature to prepare AuNP/MoS_2/MWCNT/GCE. Then, 8 μL mixed solution containing 20 mg mL^{-1} GOD and 0.25% chitosan was coated on the AuNP/MoS_2/MWCNT/GCE and dried at 4 °C in refrigerator to obtain GOD/AuNP/MoS_2/MWCNT/GCE.

Direct covalent modification of the GOD/AuNP/MoS_2/MWCNT/GCE with DNA was conducted according to the following procedure. Firstly, 10 μL of the AuNP solution was again applied to the surface of GOD/AuNP/MoS_2/MWCNT/GCE to give AuNP/GOD/AuNP/MoS_2/MWCNT/GCE for immobilization of probe ssDNA S1, to which 8 μL of 1.0×10^{-6} M probe HS-ssDNA (i.e. S1) was covalently attached (based on Au–thiol chemistry) for 10 h at 25 °C to obtain S1/AuNP/GOD/AuNP/MoS_2/MWCNT/GCE. Finally, the above electrode was modified with 6 μL GOD (20 mg mL^{-1}) solution to obtain the biosensor GOD/S1/AuNP/GOD/AuNP/MoS_2/MWCNT/GCE. The hybridization reaction was carried out by applying 8 μL target DNA to the GOD/S1/AuNP/GOD/AuNP/MoS_2/MWCNT/GCE and then incubating at 30 °C for 50 min. After that, the electrode was rinsed three times with buffer to remove the non-hybridized target DNA.

The procedure for DNA biosensor fabrication is illustrated in Scheme 1.

For DNA sensing, cyclic voltammetry (CV) was carried out in PBS (pH 6.0) containing 0.9% NaCl between −0.7 V and 0 V at a scan rate of 100 mV s^{-1}.

3. Results and discussion

3.1. Characterization of MoS_2/MWCNT composites

The MoS_2/MWCNT composites were prepared by a hydrothermal method. Fig. 1A–C displays the SEM images of MoS_2, MWCNT and MoS_2/MWCNT composites, respectively. The SEM image revealed few-layer flexible wrinkled sheets of the MoS_2 (Fig. 1A), illustrating the flakelike shape of MoS_2. The SEM image of MWCNT is shown in Fig. 1B. Many nanocarbon tubes with diameters ranging from 20 to 30 nm were observed. Fig. 3C shows the SEM image of the as-prepared MoS_2/MWCNT composites, illustrating a 3D architecture that MWCNT insert and entwine the layered MoS_2 nanosheets. The 3D architecture was helpful to increase the specific area of the composites. Furthermore, the overlapping or coalescing of the MoS_2 in the 3D MoS_2/MWCNT composites would form an interconnected conducting network, and provided a feasible pathway for electron transfer. These properties would permit the construction of an electrocatalytic platform for biosensing.

In order to reveal the fine microstructure, the as-synthesized MoS_2 and MoS_2/MWCNT composites were further characterized by TEM. As shown in Fig. 1D, the MoS_2 showed the typical thin layers folded and tangled together structure. From Fig. 1E, MWCNT was clearly observed to have been inserted and entwined the layered MoS_2 nanosheets. In the preparation process, MWCNT served as the substrate for the nucleation and growth of MoS_2 into a layered structure. On another hand, the intervention of MWCNT disturbed the well-growth of MoS_2 layered crystal structure, resulting in formation of the few-layer MoS_2, which had positive effects on the improvement in the electrochemical performances of MoS_2/MWCNT hybrid as electrochemical material.

FT-IR measurement was carried out between 4000 and 400 cm^{-1} in order to obtain the bending and stretching vibrations of functional groups present on the MoS_2 and MoS_2/MWCNT. There was no significant difference between the spectra with respect to the wavenumber of major bands for the MoS_2 and MoS_2/MWCNT composites as shown in Fig. 1F. The bands at 3400 cm^{-1} and 1240 cm^{-1} appeared at both MoS_2 and MoS_2/MWCNT FT-IR spectra were mainly assigned to stretching vibrations of the O-H bonds, and the peak at 1620 cm^{-1} was attributed to C=C stretching deformation of quinoid. The weak peak at about 600 cm^{-1} was assigned to Mo–S vibration Li and Li, 2004).

For further characterization of the as-prepared materials, the XRD pattern of MWCNT, MoS_2 and the MoS_2/MWCNT composites was recorded (Fig. 1G). It could be seen that diffraction of MoS_2 alone showed the typical crystalline peaks at 14.8°, 33°, 40° and 59°, which correspond to (002), (100), (103), and (110) planes of MoS_2 (JCPDS No. 37-1492), respectively (Liu et al., 2012). The diffraction of MWCNT showed crystalline peaks at 25.9° (002) and 42.8° (100), which attributed to the hexagonal graphite structure, indicating MWCNT had high electrical conductivity. The main diffraction peaks of MoS_2 were observed in the XRD pattern of the MoS_2/MWCNT composites. However, the major diffraction peaks of MWCNT showed very weak, indicating MoS_2 nanosheets densely covered on the surface of MWCNT. The poor crystallinity of MoS_2 was attributed to the incorporation of the MWCNT inhibited the growth of the layered MoS_2 crystal during the hydrothermal process.

Further insights of the structural and electronic properties of composites were obtained from Raman spectrum (Fig. 1H). The Raman spectrum of MWCNT exhibited the *D* band at 1342 cm^{-1} that arose from sp3-hybridized carbon, and the *G* bands at 1586 cm^{-1} which represented the E_{2g} zone center mode of the crystalline graphite. The MoS_2/MWCNT composites showed the characteristic bands at 357.3 cm^{-1} and 409.2 cm^{-1}, which were assigned to the E_{2g} and A_{1g} peaks of the MoS_2 and then the 1342 cm^{-1} and 1586 cm^{-1} bands as observed in the spectrum of MWCNT, confirming the presence of the MWCNT and MoS_2 in the composites. These results were also in agreement with the findings in the XRD diffraction studies.

TGA measurement was carried out to study the thermal stability of MoS_2, MWCNT, and MoS_2/MWCNT composites (Fig. 1I). All materials above showed an initial weight loss at approximately 100 °C, which was attributed to the evaporation of surface adsorbed water molecules. For the MoS_2, the weight loss of 27% from 100 to 410 °C was associated with water in the MoS_2 nanosheets. For the MWCNT, it exhibited approximate one-step degradation procedure. The initial degradation temperature was at about 350 °C. For the MoS_2/MWCNT composites, the decomposition temperature of 100–410 °C was attributed to the loss of co-intercalated water molecules. The weight loss of 32% in the temperature range of 410–625 °C was related to the degradation and decomposition of MWCNT. It was obvious the thermal stability of the MoS_2/MWCNT composites was better than MWCNT.

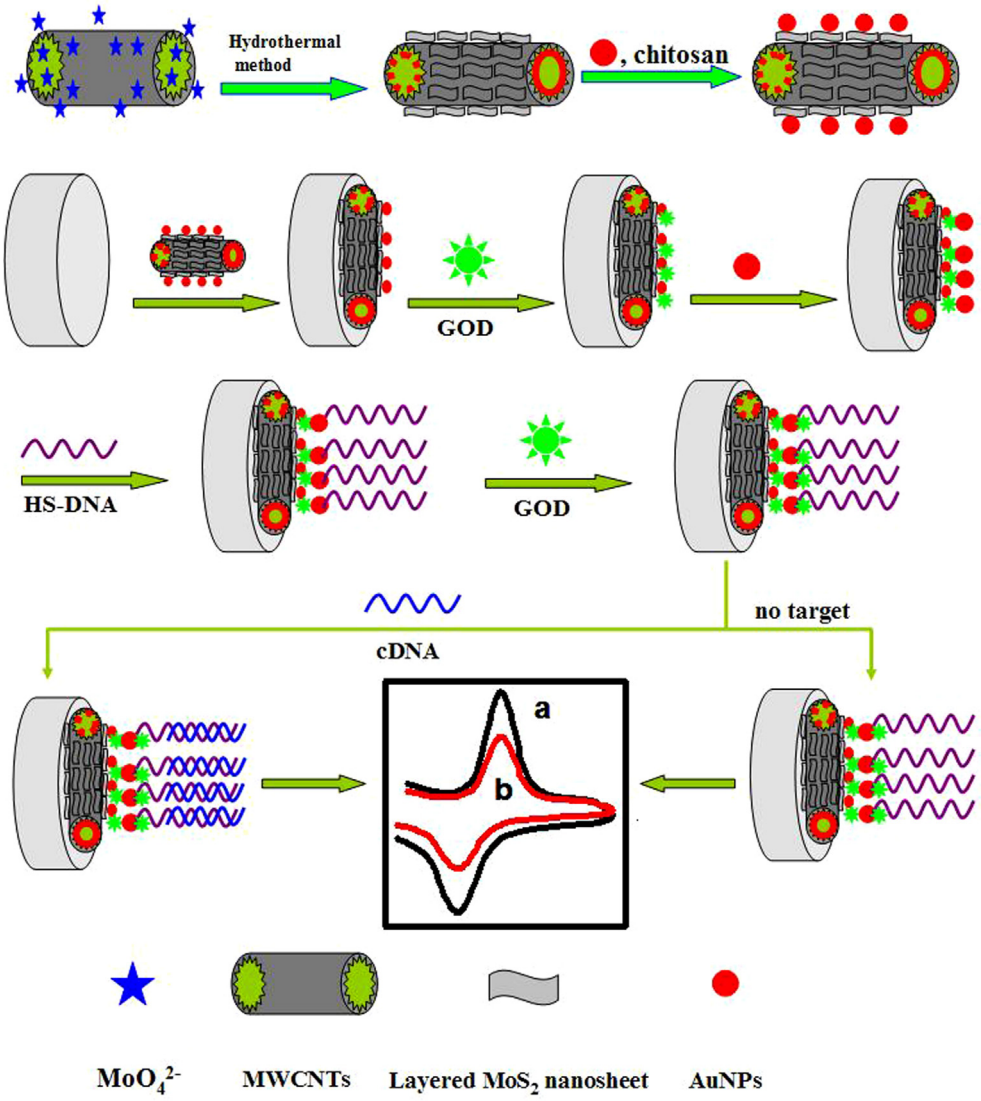

Scheme 1. Schematic diagram of the electrochemical DNA biosensor.

3.2. Electrochemical characterization

CV was used to characterize the different electrodes (Fig. 2A). The CV at the bare GCE electrode showed the lowest peak current of 24 μA (curve a). The presence of MWCNT on the bare electrode yielded a peak current of 42 μA (curve b) due to a reduced electron transfer resistance. When a MoS_2/MWCNT film was immobilized on the electrode, a corresponding peak current of 102 μA (curve c) was observed due to the good conductor of the MoS_2/MWCNT composites for accelerating the electron transfer. The results proved that the good electrochemical performance of the MoS_2/MWCNT composites.

The CVs of GOD at different modified electrodes in 0.1 M PBS (pH 6.0) containing 0.9% NaCl are shown in Fig. 2B. No obvious redox peak was observed at AuNP/MoS_2/MWCNT/GCE (curve a). After the immobilization of GOD, a pair of well defined oxidation peak at −0.37 V and reduction peak at −0.45 V, attributable to the redox reaction between FAD and $FADH_2$, was observed (curve b). In this experiment, a peak current ratio (r) of reduction peak to that at GOD/AuNPs/MoS_2/MWCNTs/GCE was estimated. At AuNP/GOD/AuNP/MoS_2/MWCNT/GCE, a corresponding r of 1.06 was obtained (curve c), suggesting the formation of electron transfer tunnels by AuNP that facilitated electron transfer. However, the r was reduced to 0.63 after S1 was attached to the electrode (curve d). This was likely to have arisen from blockage by the large oligonucleotides for electron transfer on the electrode. Subsequently, when the biosensor was blocked by GOD, the r value obviously increased to 0.78 (curve e). Following the hybridization between ssDNA and the target DNA, a dramatic decrease in r to 0.48 was observed (curve f), attributing to the form of DNA double-stranded structure retardation of the electron transfer tunnel. The results proved that the biosensor worked indeed as described in the principle scheme.

3.3. Optimization of the experiment conditions

To obtain excellent analytical performance, several experimental conditions were optimized. The GOD concentration was an important parameter affecting the signal readout. As shown in Fig. 3A, with the increasing concentration of GOD, the electrochemical response rose gradually and then tended to a constant value at 20 mg mL^{-1}, which was chosen as the optimized GOD concentration.

The pH values of PBS played the key role during the procedure of electrochemical detection since the activity of the immobilized GOD was pH dependent. As demonstrated in Fig. 3B, the electrochemical

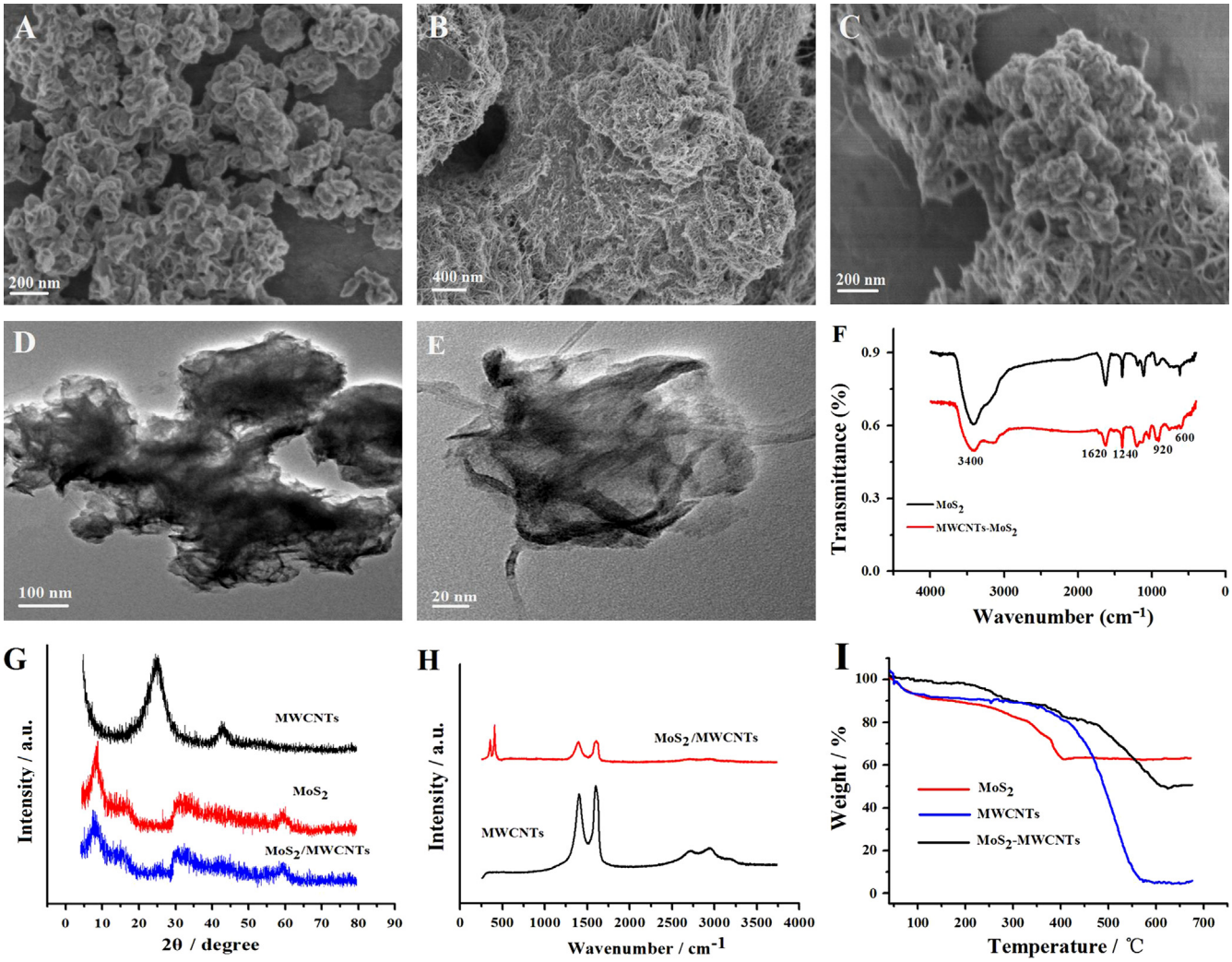

Fig. 1. SEM images of MoS_2 nanosheets (A), MWCNT (B) and MoS_2/MWCNT composites (C); TEM images of MoS_2 nanosheets (D) and MoS_2/MWCNT composites (E); FT-IR spectra of MoS_2 nanosheets and MoS_2/MWCNT composites (F); XRD patterns of MoS_2 nanosheets, MWCNT and MoS_2/MWCNT composites (G); Raman spectra of MWCNT and MoS_2/MWCNT composites (H); and TGA plots of the MoS_2, MWCNT, and MoS_2/MWCNT composites at a heating rate of 10 °C min^{-1} under N_2 atmosphere (I).

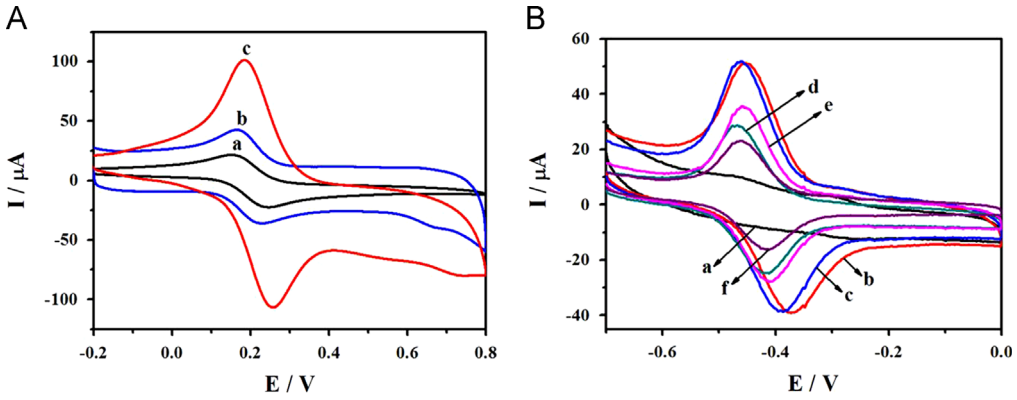

Fig. 2. (A) CVs of different electrodes in 1.0 mM $[Fe(CN)_6]^{3-/4-}$ containing 0.1 M KCl with the frequency sweep from 10^4 to 0.1 Hz: (a) bare GCE, (b) MWCNT/GCE, and (c) MoS_2/MWCNT/GCE; (B) CVs of different electrodes in 0.1 M PBS (pH 6.0) containing 0.9% NaCl: (a) AuNP/MoS_2/MWCNT/GCE, (b) GOD/AuNP/MoS_2/MWCNT/GCE, (c) AuNP/GOD/AuNP/MoS_2/MWCNT/GCE, (d) S1/AuNP/GOD/AuNP/MoS_2/MWCNT/GCE, (e) GOD/S1/AuNP/GOD/AuNP/MoS_2/MWCNT/GCE, and (f) S2/GOD/S1/AuNP/GOD/AuNP/MoS_2/MWCNT/GCE.

response increased with the increasing of pH value from 4.0 to 6.0 and reached the maximum at pH 6.0. A decrease in the electrochemical response was observed when the pH value was more than 6.0. Thus, a pH 6.0 of 0.1 M PBS solution was used in subsequent studies.

The temperature and duration of probe ssDNA covalently immobilized on the AuNP/GOD/AuNP/MoS_2/MWCNT/GCE by the Au–thiol chemistry affected the electrochemical performance of the proposed sensor for detection DNA target. The effects of these two factors on the electrochemical response were investigated.

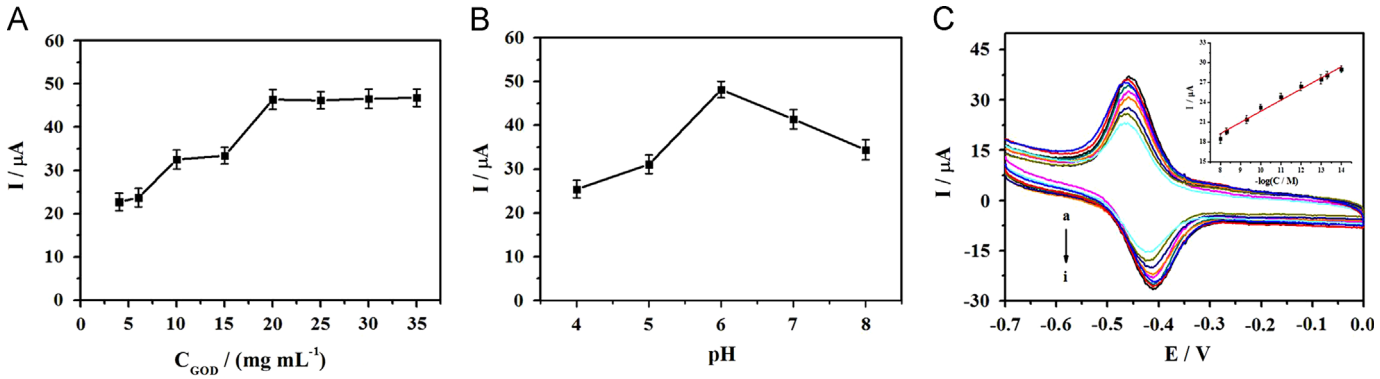

Fig. 3. The effect of the concentration of immobilized GOD (A) and pH value of the substrate solution (B) on the amperometric responses; (C) the CVs of the proposed aptasensor after incubation in different concentrations of target ssDNA standard solution (from a to i): 0.00001, 0.00005, 0.0001, 0.001, 0.01, 0.1, 0.5, 5 and 10 nM under the optimal conditions. The inset is the calibration plots for target ssDNA with the proposed DNA biosensor.

Table 1
Comparison between the proposed sensor and other sensor for DNA detection.

Electrodes	Analytical technique	Linear range (nM)	LOD (pM)	References
Ph–NH_2/GO/GCE	EIS	0.001–100	0.11	Hu et al. (2012)
Gr–AuNPs/GCE	Amperometric current–time curve	0.00005–100	0.0034	Liu et al. (2013)
Gr/polyaniline/GCE	DPV	0.0001–700	0.032	Du et al. (2012)
CeO_2–SWNTs–$BMIMPF_6$/GCE	EIS	0.001–100	0.23	Zhang et al. (2009)
CS–CeO_2–ZrO_2/Au	DPV	0.000163–16.3	0.1	Wang et al. (2012)
CeO_2/CS/GCE	DPV	0.0159–116	10	Feng et al. (2006)
4-ATP/AuNPs/Au	DPV	0.014–2	9.5	Li et al. (2012)
GOD/AuNPs/MoS_2/MWCNTs/GCE	CV	0.00001–10	0.00079	This work

Ph, Phenylenediamine; SWNT, single-walled carbon nanotubes; 4-ATP: 4-aminothiophenol; BMIMPF6, 1-butyl-3-methylimidazolium hexafluorophosphate.

The results showed that the change in electrochemical response increased along with the increase of the reaction temperature in the range of 0–25 °C, and then decreased from 25 °C to 50 °C. So the temperature of 25 °C was chosen. The change in electrochemical response was intensified when reaction time increased from 0 to 10 h, and tended to a stable value when further increases the time. Thus, 10 h reaction time was used in all subsequent works.

The hybridization temperature and time were also evaluated. The experiments were conducted by placing GOD/S1/AuNP/GOD/AuNP/MoS_2/MWCNT/GCE in DNA target solution for 20, 30, 40, 50, 60, 70 °C, respectively, and then recording the electrochemical signal. The results showed that the largest change in electrochemical signal occurred at 30 °C hybridization temperature. Similarly, the experiments were carried out at different hybridization time (0, 30, 40, 50, and 60 min) at 30 °C. The result demonstrated that the change in electrochemical signal increased gradually from 0 to 50 min, and then slightly decreased. Therefore, the hybridization conditions were chosen as 30 °C and 50 min.

3.4. Analytical performance of designed biosensor

Under the optimal experimental conditions, the CVs obtained after immobilizing synthetic target oligonucleotides of different concentration at the GOD/S1/AuNP/GOD/AuNP/MoS_2/MWCNT/GCE are shown in Fig. 3C. The reduction peak currents linearly decreased with the logarithm of target DNA concentration (10–10^7 fM), and the corresponding regression equation was i_p (μA)= 5.51–1.71 × log C (M) with a correlation coefficient of 0.991. The detection limit of this method, estimated as three times the standard deviation of the blank sample measurements, was about 0.79 fM. Compared to other methods reported previously for the detection of DNA (Table 1), the electrochemical DNA biosensor based on MoS_2/MWCNT composites, GOD and AuNP multiple signal amplification strategy showed significant improvement of the detection limit (Hu et al., 2012; Liu et al., 2013; Du et al., 2012; Zhang et al., 2009a,b; Wang et al., 2012; Feng et al., 2006; Li et al., 2012). These results revealed that MoS_2/MWCNT composites as carrier not only increased the immobilization of GOD, but also facilitated the electron transfer. In addition, the double layers of GOD membrane greatly enhanced the electrochemical signal, which improved the sensitivity of the biosensor.

The specificity of the developed DNA biosensor was investigated. Fig. 4A shows the CV signals at the GOD/S1/AuNP/GOD/AuNP/MoS_2/MWCNT/GCE before and after hybridization with different DNA targets, including the complementary sequence, the one-based mismatch sequence, the three-base mismatched sequence, and the noncomplementary sequence. A couple large redox peaks with I_{pa} of 29.5 μA and I_{pc} of 28.2 μA were observed at GOD/S1/AuNP/GOD/AuNP/MoS_2/MWCNT/GCE (curve a), indicating good electrochemical performance of AuNP/MoS_2/MWCNT composites film. After the ssDNA probe hybridized with the complementary sequence of S2, the I_{pa} decreased to 18.7 μA (curve e), which indicated that the formation of double-helix DNA. When the noncomplementary sequence of S5 was hybridized, the change in the peak current (curve b) was little (I_{pa}=27.1 μA) compared with that of the ssDNA probe-modified electrode, which indicated that the hybridization reaction was not achieved for S5. The specificity of the sensor was also evaluated by hybridization with the one-base mismatched sequence of S3 (curve d) and the three-base mismatched sequence of S4 (curve c). The result showed that peak current for three-base mismatched DNA (I_{pa}=24.6 μA) was diminished relative to that on GOD/S1/AuNP/GOD/AuNP/MoS_2/MWCNT/GCE, but was still significantly higher than that obtained from hybridization with S2 (18.7 μA). On the other hand, the peak current for one base mismatched DNA sequence was higher (I_{pa}=24.6 μA) than the complementary sequence but lower than

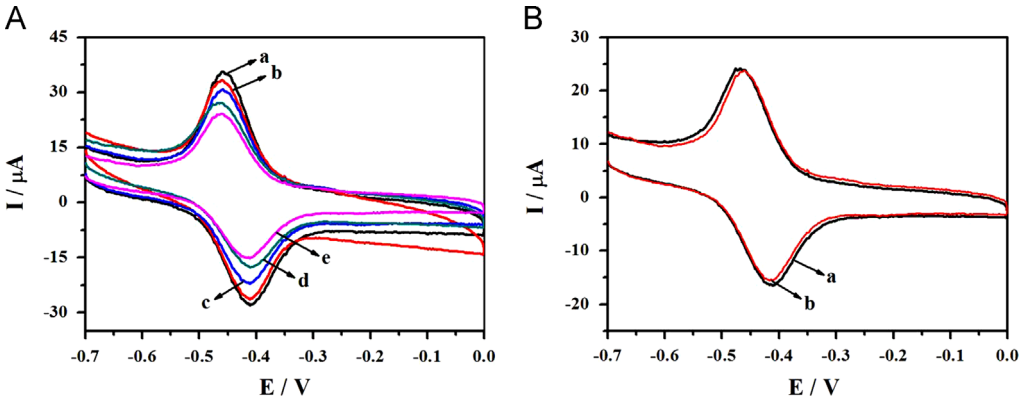

Fig. 4. (A) CVs of GOD/S1/AuNP/GOD/AuNP/MoS_2/MWCNT/GCE (a) and its hybridization with 1.0×10^{-11} mol L^{-1} different S2 sequence 0.1 M PBS (6.0) containing 0.9% NaCl: noncomplementary sequence (b), three-based mismatch sequence (c), single-based mismatch sequence (d), and complementary sequence (e); (B) one cycle (a) and 50 cycles (b) of CV measurements in 0.1 M PBS (pH 6.0) containing 0.9% NaCl after hybridization with complementary ssDNA sequence.

the three-base mismatched DNA. These results indicated that the developed biosensor had high selectivity and efficiency for the hybridization detection.

3.5. The precision and stability of the DNA biosensor

The precision and stability of the fabricated biosensor were investigated. In the precision study, the reproducibility (intra-assay) and repeatability (inter-assay) of the developed biosensor were tested at three different concentrations of target DNA (0.05, 0.5 and 5 pM). Intra-assays of the three samples were performed in three duplicates with the same biosensor and inter-assays with different biosensors using the same manufactured batch. For intra-assays, the relative standard deviation (RSD) varied from 2.1% to 4.8%, while that for inter-assay varied from 2.5% to 3.6%, indicating the fabrication procedure of the developed biosensor was reliable.

The stability of the DNA sensor was studied by measuring its cyclic voltammetric response at the electrode in pH 6.0 PBS. The results obtained using 0.1 pM complementary oligonucleotide are shown in Fig. 4B. After fifty successive scans, the RSDs were found to be 3.2%. The longtime stability of the modified electrode was also studied on a 15-day period. The cyclic voltammetric responses of the DNA sensors were compared to those obtained on the first day. An average response decrease of 1.8% was observed after 3 days, 2.8% after 10 days and 3.9% after 15 days. This good stability was mainly attributed to the AuNP/MoS_2/MWCNT composites film which possessed excellent environmental and chemical stability.

3.6. Detection of serum samples

The developed method was used to detect the target DNA in serum samples. Firstly, the serum sample was diluted to 1:10 with PBS (pH 6.0). 0.1 M PBS (pH 6.0) and the serum sample were then spiked with three target DNA concentrations (0.01 pM, 10 pM, 6.5 nM), respectively, and the reduction peak current was recorded at the GOD/S1/AuNP/GOD/AuNP/MoS_2/MWCNT/GCE. The peak current of three spiked target DNA concentrations was close in serum (19.3, 23.1, and 28.7 μA) and in 0.1 M PBS (19.5, 23.8, and 29.3 μA), indicating good potential of the developed assay for clinical applications.

4. Conclusion

In summary, we have developed a simple and ultrasensitive electrochemical DNA biosensing method for convenient detection of specific DNA sequence through integrating MoS_2/MWCNT composites and AuNP signal amplification with enzymatic signal readout. The MoS_2/MWCNT composites film possessed large specific surface area and excellent biocompatibility, which not only increased the immobilization of GOD, but also retained the active immobilized biomolecules and enhanced the stability of the DNA probe. In addition, the double layer GOD membranes as tracer brought about higher current response and higher sensitivity. The proposed DNA sensor showed relatively low detection limit (0.79 fM), wide linear range (10 M to 10^7 fM) and satisfactory selectivity, and it would be attractive for genetic target analysis in bioanalytical and clinic biomedical application.

Acknowledgments

This work was supported by the National Natural Science Foundation of China (U1304214 and 21375114) and Program for University Innovative Research Team of Henan (2012IRTSHN017).

References

Babaei, A., Taheri, A.R., 2013. Sensors Actuat. B: Chem. 176, 543–551.
Batra, B., Pundir, C.S., 2013. Biosensors Bioelectronics 47, 496–501.
Du, M., Yang, T., Li, X., Jiao, K., 2012. Talanta 88, 439–444.
Feng, K.J., Yang, Y.H., Wang, Z.J., Jiang, J.H., Shen, G.L., Yu, R.Q., 2006. Talanta 70, 561–565.
Feng, J., Sun, X., Wu, C.Z., Peng, L.L., Lin, C.W., Hu, S.L., Yang, J.L., Xie, Y., 2011. J. Am. Chem. Soc. 133, 17832–17838.
Gao, F.L., Zhu, Z., Lei, J.P., Geng, Y., Ju, H.X., 2013. Biosensors Bioelectronics 39, 199–203.
Hwang, H., Kim, H., Cho, J., 2011. Nano Lett. 11, 4826–4830.
Hu, B.L., Qin, X.Y., Asiri, A.M., Alamry, K.A., Al-Youbi, A.O., Sun, X.P., 2013. Electrochem. Commun. 28, 75–78.
Hu, Y.W., Li, F.H., Han, D.X., Wu, T.S., Zhang, Q.X., Niu, L., Bao, Y., 2012. Anal. Chim. Acta 753, 82–89.
Huang, J., Wu, Y.R., Chen, Y., Zhu, Z., Yang, X.H., Yang, C.Y.J., Wang, K.M., Tan, W.H., 2011. Angew. Chem. Int. Ed. 50, 401–404.
Huang, K.J, Wang, L., Li, J., Liu, Y.M., 2013a. Sensors Actuat. B: Chem. 178, 671–677.
Huang, K.J., Wang, L., Liu, Y.J., Wang, H.B., Liu, Y.M., Wang, L.L., 2013b. Electrochim. Acta 109, 587–594.
Huang, K.J., Wang, L., Liu, Y.J., Gan, T., Liu, Y.M., Wang, L.L., Fan, Y., 2013c. Electrochim. Acta 107, 379–387.
Jiang, Y., Zhao, H., Zhu, N.N., Lin, Y.Q., Yu, P., Mao, L.Q., 2008. Angew. Chem. Int. Ed/ 47, 8601–8604.
Karadas, N., Bozal-Palabiyik, B., Uslu, B., Ozkan, S.A., 2013. Sensors Actuat. B: Chem. 186, 486–494.
Li, J., Yang, Z.j., Tang, Y., Zhang, Y.C., Hu, X.Y., 2013. Biosensors Bioelectronics 41, 698–703.
Li, G.J., Liu, L.H., Qi, X.W., Guo, Y.Q., Sun, W., Li, X.L., 2012. Electrochim. Acta 63, 312–317.
Li, X.L., Li, Y.D., 2004. J. Phys. Chem. B 37, 13893–13900.
Ling, S.J., Yuan, R., Chai, Y.Q., Zhang, T.T., 2009. Bioprocess Biosyst. Eng. 32, 407–414.
Liu, A.L., Zhong, G.X., Chen, J.Y., Weng, S.H., Huang, H.N., Chen, W., Lin, L.Q., Lei, Y., Fu, F.H., Sun, Z.L., Lin, X.H., Lin, J.H., Yang, S.Y., 2013. Anal. Chim. Acta 767, 50–58.
Liu, S.S., Zhang, X.B., Shao, H., Xu, J., Chen, F.Y., Feng, Y., 2012. Mater. Lett. 73, 223–225.

Liu, X.Q., Freeman, R., Golub, E., Willner, I., 2011. ACS Nano 5, 7648–7655.
Ma, G.F., Peng, H., Mu, J.J., Huang, H.H., Zhou, X.Z., Lei, Z.Q., 2013. J. Power Sources 229, 72–78.
Rezaei, H., Ardakani, S.J., Smith, K.J., 2012. Energy Fuels 26, 2768–2778.
Sui, J., Zhang, L.J., Peng, H., 2013. Eur. Polym. J. 49, 139–146.
Tang, L.H., Liu, Y., Ali, M.M., Kang, D.K., Zhao, W.A., Li, J.H., 2012. Anal. Chem. 84, 4711–4717.
Wan, Y., Xu, H., Su, Y., Zhu, X.H., Song, S.P., Fan, C.H., 2013. Biosensors Bioelectronics 41, 526–531.
Wang, G.X., Bao, W.J., Wang, J., Lu, Q.Q., Xia, X.H., 2013a. Electrochem. Commun. 35, 146–148.
Wang, Li., Hua, E.H., Liang, M., Ma, C.X., Liu, Z.L., Sheng, S.C., Liu, M., Xie, G.M., Feng, W.L., 2014. Biosensors Bioelectronics 51, 201–207.
Wang, Q.X., Gao, F., Zhang, X., Zhang, B., Li, Sh.X., Hu, Z.S., Gao, F., 2012. Electrochim. Acta 62, 250–255.
Wang, W., Song, L., Gao, Q., Qi, H.L., Zhang, C.X., 2013b. Electrochem. Commun. 34, 18–21.
Yao, W., Wang, L., Wang, H.Y., Zhang, X.L., Li, L., Zhang, N., Pan, L., Xing, N.N., 2013. Biosensors Bioelectronics 40, 356–361.
Yin, X.B., 2012. Trends Anal. Chem. 33, 81–94.
Zhang, W., Yang, T., Zhuang, X., Guo, Z., Jiao, K., 2009a. Biosensors Bioelectronics 24, 2417–2422.
Zhang, X.F., Luster, B., Church, A., Muratore, C., Voevodin, A.A., Kohli, P., Aouadi, S., Talapatra, S., 2009b. ACS Appl. Mater. Interfaces 1, 735–739.
Zhou, L., Wang, J.P., Gai, L., Li, D.J., Li, Y.B., 2013. Sensors Actuat. B: Chem. 181, 65–70.